Environ Monit Assess (2021) 193: 464
https://doi.org/10.1007/s10661-021-09220-w

Assessing lodging damage of jute crop due to super cyclone *Amphan* using multi-temporal Sentinel-1 and Sentinel-2 data over parts of West Bengal, India

Abhishek Chakraborty · P. Srikanth · C. S. Murthy · P. V. N. Rao · Santanu Chowdhury

Received: 4 January 2021 / Accepted: 12 June 2021 / Published online: 4 July 2021

Abstract The present study is a maiden attempt to assess jute crop lodging due to super cyclone *Amphan* (20 May 2020) by synergistic use of Sentinel-2 (optical) and Sentinel-1 (SAR) data over part of West Bengal, India. Pre-event Sentinel-2 data (9 April, 14 May) along with the ground information were used to map the jute crop of the affected districts with accuracy of 85%. The cross-polarized backscatter (σ^0_{VH}) of Sentinel-1 was found to be sensitive to the sudden change in the canopy structure due to lodging and partial flooding. $\triangle\sigma^0_{VH}(\sigma^0_{VH\_22\ May} - \sigma^0_{VH\_16\ May})$ indicating post-event damage was > 2.5 dB over the affected jute crop and $\delta\sigma^0_{VH}$ $(\sigma^0_{VH\_22\ May} - \sigma^0_{VH\_28\ May})$ representing post-event recovery showed > 1.5 dB for recovered crop, depending on the crop vigor/height. Decision matrix was prepared combining $\triangle\sigma^0_{VH}$ and $\delta\sigma^0_{VH}$ for NDVI-based crop vigor strata (low, medium, and high) to classify the area into affected, marginally affected and normal. Overall accuracy of the classified map was found to be 84.12% with kappa coefficient of 0.74. Nearly, 12.5% of the jute area, i.e., 38,119 ha was found to be either affected or marginally affected due to *Amphan* and distributed in the southern part of Murshidabad, north-eastern Nadia, northern 24 Paraganas (N), and middle region of Hooghli district. Geospatial map of block-wise affected jute area was prepared to facilitate informed decision making. The study demonstrated an operational methodology for assessing crop lodging due to natural calamities to support relief management and crop insurance.

Keywords *Corchorus* · Cyclone damage · Crop mapping · Crop lodging · SAR · Cross-polarized backscatter

Highlights
- Lodging damage of jute crop due to cyclone *Amphan* was assessed using multi-temporal optical and SAR satellite data
- Jute crop map was prepared based on Sentinel-2 data and ground-based observations.
- The cross polarized backscatter return of Sentinel-1 was found to be sensitive to crop lodging
- Decision matrix prepared using temporal changes in cross polarized backscatter return over different NDVI based crop strata to assess the affected jute crop

A. Chakraborty (✉) · P. Srikanth · C. S. Murthy · P. V. N. Rao · S. Chowdhury
Agro-Ecosystem and Modeling Division, Agricultural Sciences and Applications Group, National Remote Sensing Centre, Indian Space Research Organization, Hyderabad, India
e-mail: jeet.abhishek@gmail.com

Introduction

Tropical super cyclonic storm "*Amphan*" made landfall on West Bengal near the *Sundarbans* (mangrove forest) between Digha and Hatiya at 1430 h IST (0900 h UTC) on May 20, 2020, buffeting the region with strong winds and heavy rains. West Bengal being the epicenter of the cyclone landfall saw

the most widespread damage from Amphan. The storm was considered to be the strongest to hit the region over a decade. The southern districts of West Bengal particularly South and North 24 Paraganas, Howrah, Hooghly, Kolkata, Nadia, East and West Midnapur, parts of Murshidabad and Burdwan were highly affected. There has been a widespread damage of the standing jute and other crops particularly over the southern districts due to inundation and lodging of the crops. Such cyclonic storms originated from Indian Ocean are regular phenomenon and cause damage to the standing crops. So an operational procedure is need of the hour to objectively assess the cropped area affected due to cyclonic storm for informed rehabilitation and compensation to the farmers.

Crop lodging can be described as displacement of crop stems from its vertical or upright position or failure from anchorage of root-soil (Pinthus, 1974). It is one of the important yield-reducing factors of crops (Islam et al., 2007; Wu & Ma, 2016). It is also a complex phenomenon mainly governed by the crop genetic factors, prevailing environmental condition and crop management. Thus, every crop lodging is unique in terms of its onset, intensity, and persistence (Piñera-Chavez et al., 2016; Zhu et al., 2016). Traditionally, assessment of crop lodging is done using in situ visual rating or sophisticated field/lab-based modeling (Baker et al., 2014; Berry et al., 2004; Brune et al., 2018; Mi et al., 2011). But this approach lacks scalability as it is point-based, data intensive, complex, and computationally expensive.

Remote sensing (RS) technique offers a relatively simple, inexpensive alternative to assess crop lodging over a large area in near-real time. Considerable efforts have been made to use remote sensing techniques to assess crop lodging using field-level proximal sensing, airborne, and space-borne sensors. Chauhan et al. (2019) made a comprehensive review on such efforts of remote sensing-based crop lodging assessment. These efforts mainly directed towards detection and estimation of changes of crop biophysical (leaf area index, crop height, biomass, etc.) and biochemical parameters (greenness, chlorophyll content, moisture content, etc.) due to crop lodging. Ground-based measurements involve multispectral or hyperspectral sensors in optical region to estimate the changes in spectral indices, pixel contrast, brightness, etc. attributing to crop lodging (Constantinescu et al., 2017; Liu et al., 2011; Ogden et al., 2002; Sakamoto et al., 2010). Ground-based X-band scatterometer has also been used at different polarizations and incident angles to assess lodging of potato, wheat, barley, and oats (Bouman, 1991; Bouman & van Kasteren, 1990a, b).

Recent advancements of remotely piloted aircraft system (RPAS) along with robotics, electronics, and computer vision usher new opportunities in the field of airborne remote sensing (Nebiker et al., 2008). Fine spatial resolution and real-time monitoring ability of airborne RS system is well suited for periodic monitoring of crop attributes and post-disaster assessment such as crop lodging (Ezequiel et al., 2014). Zhang et al. (2014) conducted quantitative analysis of crop lodging using airborne sensors and reported high contrast between lodged and normal crop in infrared region. Chapman et al. (2014) further reported the sensitivity of red-edge and thermal bands in detecting lodged area. Liu et al. (2014) used spectral and textural feature of UAV-based images to classify accurately lodged and no-lodged areas. Yang et al. (2017) further used decision tree classifier to assess the lodged area combing spectral and textural image features. Chu et al. (2017) estimated number of lodged plants per unit area based on grid-based mathematical model of plant height derived from airborne VNIR sensor. Constantinescu et al. (2017) used airborne multispectral sensor and found differential spectral response between lodged and non-lodged wheat and barley crop. This has further been used to produce spatial map of normal and lodged crop using Euclidian distance-based clustering technique. Airborne platform showed the potential of RS technique towards assessing the crop lodging, but it is cost-prohibitive for regional or large-scale applications.

Studies on assessment of crop lodging over a large area using satellite data are sparse and mainly concentrated in the microwave domain for its all-weather capability. Continuous improvement of the space-based sensor technologies, systematic high-frequency coverage, and reduced cost of the satellite data unravel great potential to operationally assess crop lodging based on spaceborne RS data. Yang et al. (2015) used RADARSAT-2 SLC C-band fully

polarimetric data to assess wheat crop lodging in Inner-Mongolian region of China and demonstrated that polarimetric ratio can be used to distinguish lodged and normal field. Chen et al. (2016) used similar data over sugarcane crop in Guangdong province of China and showed that polarimetric features such as double bounce and volume scattering were capable of detecting lodging. Zhao et al. (2017) showed that RADARSAT-2-derived σ^0_{VV}, σ^0_{HH}, depolarization degree, and circular-pol correlation coefficient were highly sensitive to lodged wheat but not for canola whose canopy is highly random in nature. Han et al. (2017) used Sentinel-1 C-band VV and VH polarization to study the lodging of corn at Beijing, China. The study showed that polarization response due to height difference before and after lodging can be used to classify the degree of lodged area into mild, moderate, and severe. Similar observation was also made by Shu et al. (2020) and calculated lodging angle of maize crop with an overall accuracy of 67% using plant height inversion. Wu et al. (2019) used multi-temporal Sentinel-1 and Sentinel-2 data to assess flooding and lodging of paddy rice over Zhejiang, China, due to typhoon Maria. He proposed rice normalized difference flooded index and rice normalized difference lodged index to assess the affected area successfully. Recently, Chauhan et al. (2020a) estimated crop angle of inclination (CAI) of lodged wheat crop using multi-temporal RADARSAT-2 and Sentinel-1 SAR data. The study emphasized the importance of systematic high frequency coverage of SAR data like Sentinel-1 for operational assessment of CAI-based lodging stages with significant accuracy (78%). Continuing further, Chauhan et al. (2020b) used both Sentinel-1 (SAR) and Sentinel-2 (Optical) data to demonstrate its potential towards near real-time detection of the incidence and severity of lodging in wheat.

The present study, for the first time, used multi-temporal Sentinel-1 SAR data along with Sentinel-2 optical data to assess the lodging of jute crop due to super cyclone *Amphan*. The study is mainly focused on developing a methodology for operational near-real time assessment of crop damage (jute in present case) due to lodging and partial inundation caused by cyclonic storm. The study also accommodated post-event recovery of the crop towards assessing the crop damage.

Tracking cyclone Amphan

Low pressure area near equatorial easterly wave over south Andaman Sea and adjoining south-east Bay of Bengal during May 1–5 is the origin of *Amphan* cyclone. It has developed as a very severe cyclonic storm (VSCS) and crossed West Bengal–Bangladesh coasts, across *Sundarbans*, near latitude 21.65° N and longitude 88.30° E during 1530–1730 h IST (1000–1200 UTC) of 20 May, with maximum sustained wind speed of 155–165 km h^{-1} gusting to 185 km h^{-1}. It lay over West Bengal as a VSCS, gradually moving north-northeastward during late evening to night (1200–1500 UTC) of 20 May. It moved very close to Kolkata during this period. Moving further north-northeastward, it weakened into a severe cyclonic storm over Bangladesh and adjoining West Bengal around midnight (1800 UTC) of 20 May, weakened further into a cyclonic storm over Bangladesh in the early hours (2100 UTC of 20th) of 21 May, into deep depression over Bangladesh around noon of 21 May and into a depression over north Bangladesh in the evening (1200 UTC) of the same day. It further weakened and lay as a well-marked low-pressure area over north Bangladesh and neighborhood around mid-night (1800 UTC) of 21 May. The observed track of *Amphan* is presented in Fig. 1.

Rainfall and wind speed during cyclone *Amphan*

India Meteorological Department (IMD) receives points based sub-daily meteorological observations across India and converts it at daily level (0830 h IST of current day from 0830 h IST from previous day). It is further interpolated at 0.1° grid using suitable GIS techniques. IMD gridded (0.1°) daily average rainfall and wind speed data during 19–22 May 2020 are presented in Fig. 2. As per the data, there had been no to very little rainfall on 19 and 20 May with a prevailing daily average wind speed of 0–10 km h^{-1}. Pre-landfall rainfall of 10–50 mm per day was observed in the different parts of south Bengal with a higher daily average wind speed of 10–20 km h^{-1}. As mentioned earlier, the *Amphan* landfall took place at 1430 h IST on 20 May 2020. Hence, sudden increase in the rainfall was observed on the following day of 21 May

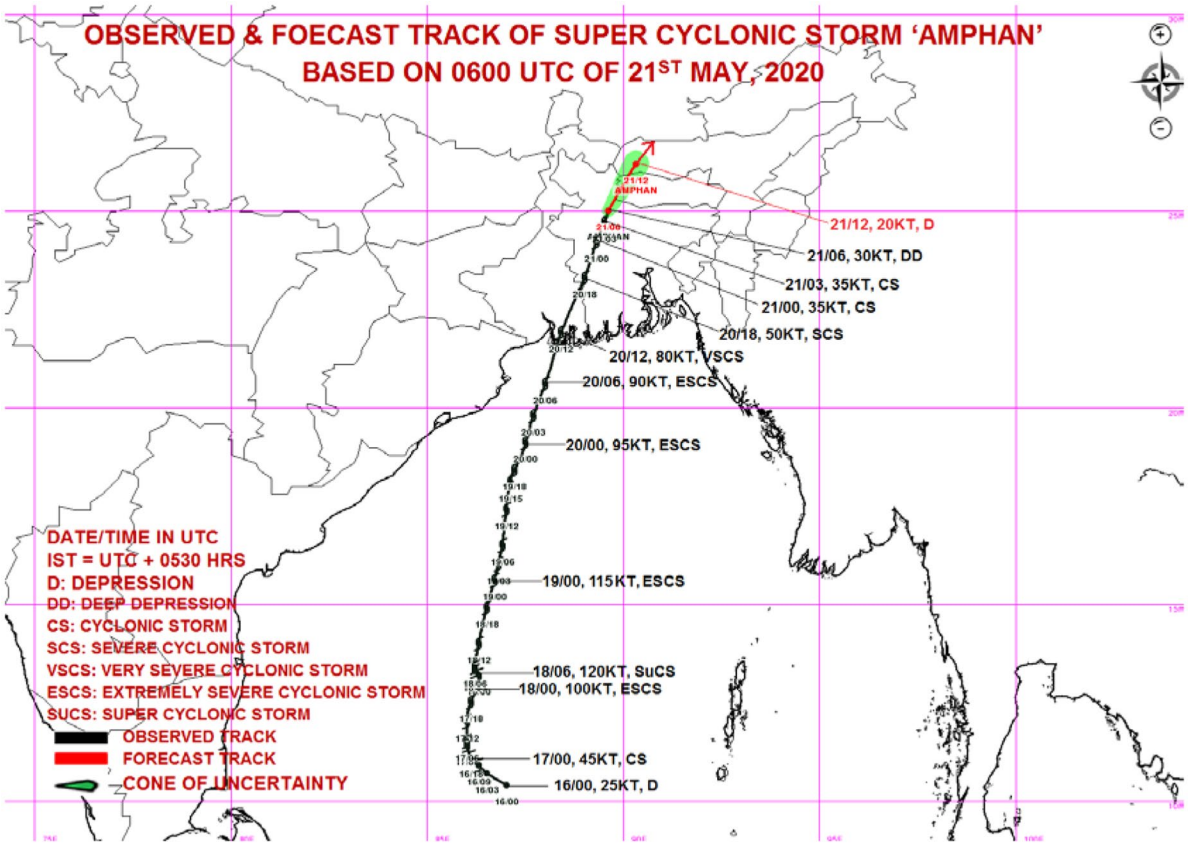

Fig. 1 Observed track of super cyclone *Amphan* as on 21 May 2020 (courtesy IMD, India)

particularly in the different districts of southern parts of West Bengal. More than 200 mm day^{-1} rainfall was observed over South and North 24 Paraganas, Howrah, Hooghli, Nadia, Kolkata, parts of Burdwan. Nearly 100–200 mm rainfall was observed over East and West Midnapur, parts of Bankura, Burdwan, and Murshidabad. At the same time, extremely high daily average wind speed was observed (40–80 km h^{-1}) over the above mentioned districts. Wind gust (short and peak wind speed) was reported by IMD to be 110–130 km h^{-1}. The rainfall activity was found to be minimal with normal daily average wind speed (0–5 km h^{-1}) on 22 May. As a result of the severe wind speed and rainfall during 20–21 May, large-scale flooding/inundation along with mechanical damage/lodging of the crops were reported across the southern district of West Bengal.

Standing crops exposed to the calamity

Indian agriculture has two major growing seasons, i.e., *kharif* or wet season (July to November) and *rabi* or dry season (December to April). Hence, month of May is a lean period of agricultural activities. *Rabi* crops are generally harvested by this time and the ensuing *kharif* season is supposed to start from June-July month. But, West Bengal being high in the cropping intensity, significant *zaid* (third) season crops existed during cyclone landfall. As per the local knowledge, the majority of the cropped area was under Jute crop during this time, followed by *Sesamum* which was near to maturity, and different vegetables like (pointed gourd, ridge gourd, etc.). Some areas of ready to harvest *boro (rabi)* rice were also reported. Jute crop is generally sown in the month

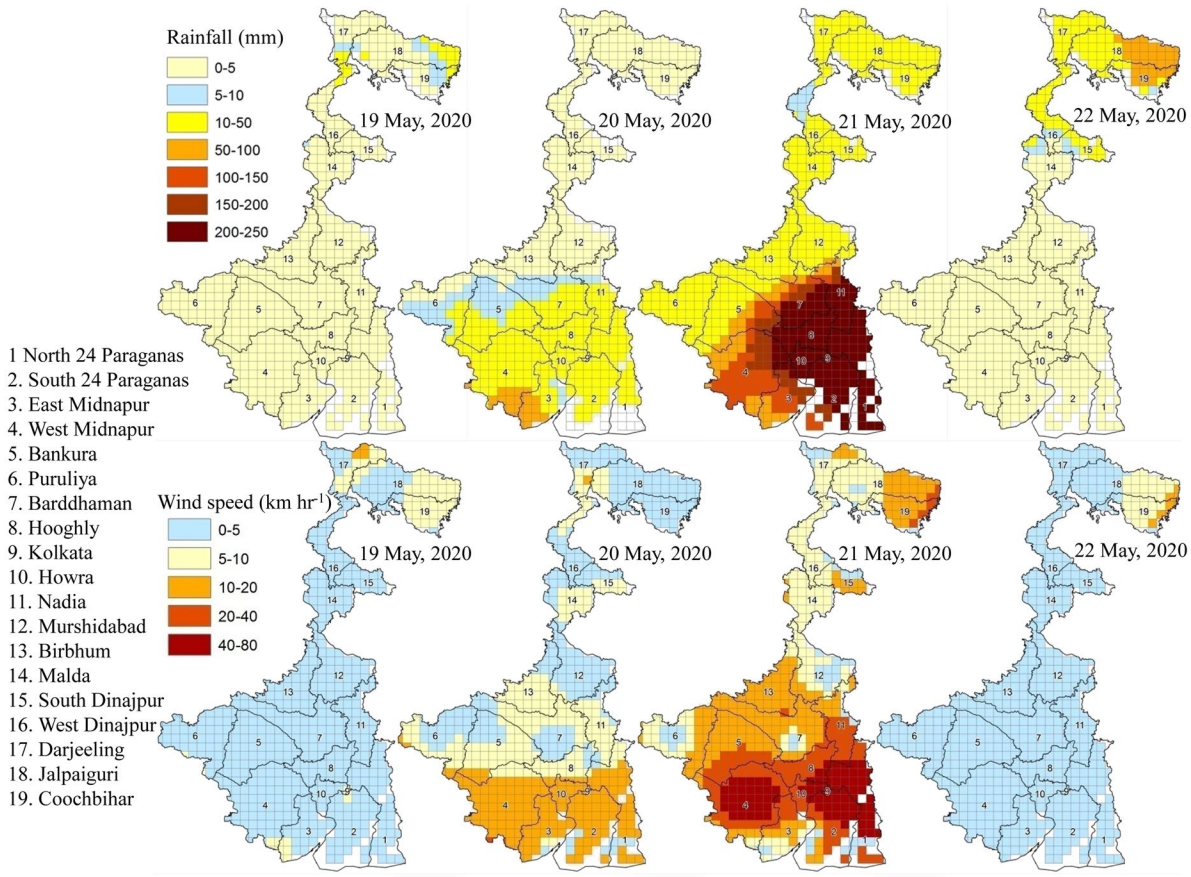

Fig. 2 India Meteorological Department (IMD) gridded rainfall and wind speed over West Bengal during 19–22 May 2020

of April synchronized with pre-monsoon shower. There had been a staggering of the sowing of jute crop. The peak of the sowing activity was observed in the second and third week of April. But in some areas, sowing took place in the first and last week of April also. So, the jute crop was found to be nearly 1 to 1.5-month-old with a height of 2–5 ft during the cyclonic storm. Representative field photographs of early and late sown jute crops are shown in Fig. 3.

Study area

Considering the track of the cyclone and area under jute crop, four districts were selected for the present

Fig. 3 Early and late sown jute crop over West Bengal as on 19 May 2020

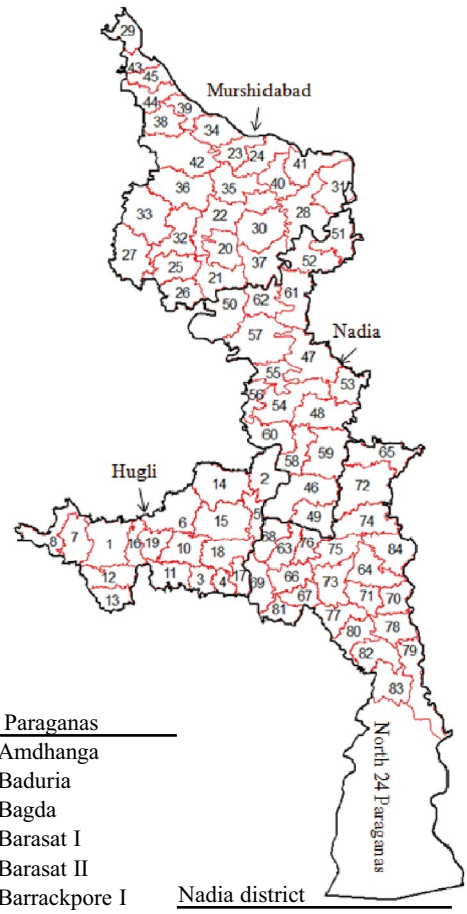

Fig. 4 Study area covering four districts (Murshidabad, Nadia, Hooghli, and North 24 Paraganas) and their block boundaries

Hughli District

1	Arambhag
2	Balagarh
3	Chanditala I
4	Chanditala II
5	Chinsurah-Magra
6	Dhaniakhali
7	Goghat I
8	Goghat II
10	Haripal
11	Jangipara
12	Khanakul I
13	Khanakul II
14	Pandua
15	Polbadarpur
16	Pursura
17	Serampur-Uttarpara
18	Singur
19	Tarakeshwar

Murshidabad district

20	Beldanga I
21	Beldanga II
22	Berhampur
23	Bhagawangola I
24	Bhagawangola II
25	Bharatpur I
26	Bharatpur II
27	Burwan
28	Domkal
29	Farakka
30	Hariharpara
31	Jalangi
32	Kandi
33	Khargram
34	Lalgola
35	Murshidabad-Jiaganj
36	Nabagram
37	Nawda
38	Raghunathganj I
39	Raghunathganj II
40	Raninagar I
41	Raninagar II
42	Sagardighi
43	Samserganj
44	Suti I
45	Suti II

North 25 Paraganas

63	Amdhanga
64	Baduria
65	Bagda
66	Barasat I
67	Barasat II
68	Barrackpore I
69	Barakpore II
70	Basirhat I
71	Basirhat II
72	Bongaon
73	Deganga
74	Gaighata
75	Habra I
76	Habra II
77	Haora
78	Hasnabad
79	Hingalganj
80	Ninakhan
81	Rajarhat
82	Sandeshkhali I
83	Sandeshkhali II
84	Swarupnagar

Nadia district

46	Chakdaha
47	Chapra
48	Hanskhali
49	Haringhata
50	Kaliganj
51	Karimpur I
52	Karimpur II
53	Krishnaganj
54	Krishnanagar I
55	Krishnanagar II
56	Nabadwip
57	Nakashipara
58	Ranaghat I
59	Ranaghat II
60	Santipur
61	Tehatta I
62	Tehatta II

study as shown in Fig. 4. These four districts, i.e., Murshidabad, Nadia, North 24 Paraganas, and Hooghli, cover nearly 60% of the jute crop area of the state. Maximum damage of jute crop has also been reported from these four districts.

Methodology

The schematic diagram of the methodology followed is presented in Fig. 5. Details are as follows:

Ground data collection

Jute Corporation of India (JCI) in collaboration with National Remote Sensing Centre (NRSC) has been systematically collecting ground truth over the jute crop area using specially designed mobile app (BHUVAN JUMP). It records the different attributes of jute crop, field photographs along with the geolocations throughout the jute growing season. Total 1563 field data points are collected over the present study area before the land fall of *Amphan* during 1 April to 20 May 2020. On the other hand, nearly 200 data points were collected during post-*Amphan* scenario (21–30 May 2020). Based on the data collected using the mobile app, it was observed that the height of the jute crop was between 2 and 5 ft during the cyclonic episode. Due to twisting action of the cyclonic wind, the jute crop was flattened and lodged severely. The situation was further aggravated by the heavy rainfall causing partial/complete inundation of the jute crop. Lodging was found to be more severe for taller jute crops and marginal effect was observed over late sown jute crop with 1–2 ft height. The continuous stagnation of water for few days has detrimental effect on jute yield and may cause failure of the crop. On the other hand, the crop could recover the lodging effect if water subsides and bright sunlight prevails. The nature of damage caused by *Amphan* to the standing jute crop is presented in Fig. 6.

Satellite data used

The present study has used two pre-event cloud-free Sentinel-2 optical data, i.e., 9 April and 14 May 2020 to classify the current year jute crop area. Due to prevailing cloudy condition during and after Amphan cyclone, time-series Synthetic Aperture RADAR (SAR) data were used to assess jute crop damage. Total six Sentinel-1 scenes spanning

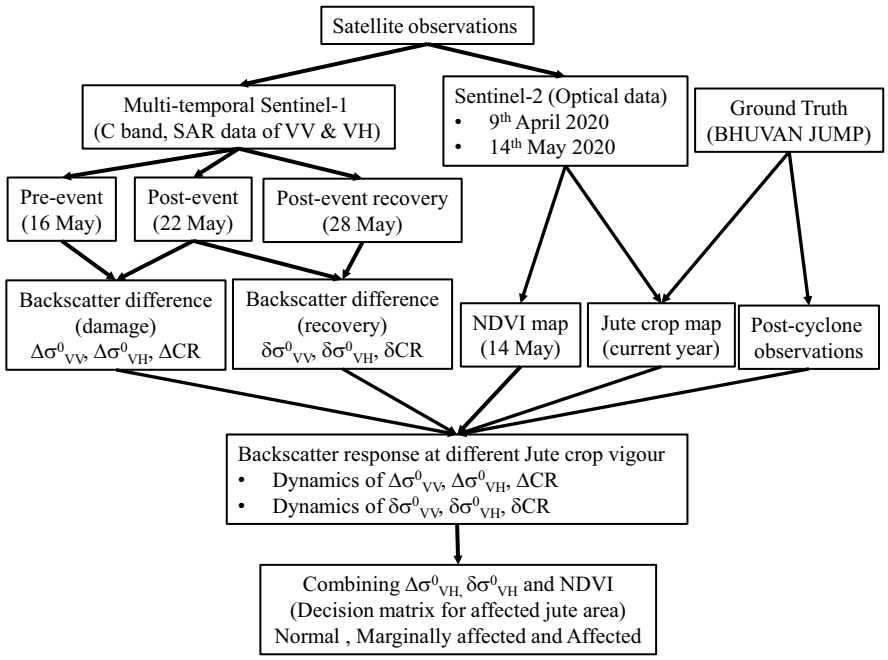

Fig. 5 The schematic diagram of the methodology followed in the present study; CR (cross-polarized ratio) $= \sigma^0_{VH}/\sigma^0_{VV}$; $\triangle\sigma^0_{VV} = (\sigma^0_{VV}$ of 22 May $- \sigma^0_{VV}$ of 16 May); $\triangle\sigma^0_{VH} = (\sigma^0_{VH}$ of 22 May $- \sigma^0_{VH}$ of 16 May); $\delta\sigma^0_{VV} = (\sigma^0_{VV}$ of 22 May $- \sigma^0_{VV}$ of 28 May); $\delta\sigma^0_{VH} = (\sigma^0_{VH}$ of 22 May $- \sigma^0_{VH}$ of 28 May); ΔCR = (CR of 22 May − CR of 16 May); δCR = (CR of 22 May − CR of 28 May)

Fig. 6 Representative photographs of jute crop damaged by *Amphan* super cyclone. **A** Lodged jute crop. **B** Lodged and inundated jute crop

throughout the jute season (4 April to 28 May 2020) were analyzed in the present study (Table 1). Time series Sentinel-1(C-band, wavelength 5.4 cm) were acquired in interferometric wide swath (IW) mode with dual polarisation (VV and VH), descending orbit (~39° incident angle) in ground range detected (GRD) format from the Copernicus Open Access (COA) Hub of the European Space Agency (ESA Standard Document, 2015).

Processing of satellite data

Sentinel-1 and Sentinel-2 data pertains to the study area were downloaded from http://scihub.copernicus.eu/dhus/ and processed as below. Cloud-free Sentinel-2 (optical) data of 9 April and 14 May 2020 were downloaded from COA Hub. The false color composite (FCC) of the Sentinel-2 images are presented in Fig. 7. Sentinel-2 optical data were used to classify jute crop as mentioned above. The Sentinel-2 data of 14 May is also used to calculate NDVI. The NDVI is calculated as the normalized difference between near-infrared and red bands, and to quantify vigor and photosynthetic capacity of crop. Hence, NDVI indicates the amount of vegetation present in one place and used to stratify jute crop into high, medium and low category of vigor.

On the other hand, Sentinel-1 SAR data were processed in SNAP 6.0 software. Radiometric calibration of the SAR data was carried out as a first step and a refined Lee filter with kernel size 7×7 was used to suppress the speckle noise in the SAR images. Range-Doppler terrain correction model was used to geometrically correct the SAR images with the help of SRTM DEM of 30 m resolution. The linear sigma naught images were converted to backscattering coefficient in dB scale. Each image consists of two polarizations, i.e., VV and VH. A layer stack of temporal VV and VH images was generated for further analysis. Cross-polarization ratio ($CR = \sigma^0{}_{VH}/\sigma^0{}_{VV}$) images were also generated for each date.

Table 1 Description of Sentinel-1 data used in the present study

Sl. no	Sensor (beam mode)	Polarization	Incidence angle mid swath (deg.)	Date of acquisition	Local time	Orbit direction
1	Sentinel-1A (IW GRD)	VV, VH	39.1	4 April 2020	6:04 am	Descending
2	Sentinel-1A (IW GRD)	VV, VH	39.1	16 April 2020	6:04 am	Descending
3	Sentinel-1A (IW GRD)	VV, VH	39.1	28 April 2020	6:04 am	Descending
4	Sentinel-1B (IW GRD)	VV, VH	39.0	16 May 2020	6:03 am	Descending
5	Sentinel-1A (IW GRD)	VV, VH	39.1	22 May 2020	6:04 am	Descending
6	Sentinel-1B (IW GRD)	VV, VH	39.0	28 May 2020	6:03 am	Descending

Combing SAR and optical data for decision matrix

Present study used six dates of SAR data as mentioned above to develop the signature of the SAR backscatter at different polarization over normal and damaged jute crop. Further, three dates of Sentinel-1 SAR data, i.e., 16 May (pre-event), 22 May (post-event), 28 May (post-event recovery), were used for assessing the lodging damage. Three metrics, i.e., $\triangle\sigma^0_{VV}$, $\triangle\sigma^0_{VH}$, and ΔCR were calculated using the Sentinel-1 images of 16 and 22 May to characterize damage due to cyclone. Whereas, three more metrics, i.e., $\delta\sigma^0_{VV}$, $\delta\sigma^0_{VH}$, and δCR were derived using the Sentinel-1 images of 22 and 28 May to characterize the post-event recovery of the crop. The NDVI values derived from pre-event (14 May) cloud-free optical data of Sentinel-2 was used to characterize the vigor of the jute crop. The dynamics of these six metrics over the different crop vigor strata were analyzed and merged into decision matrix to classify the jute area into normal, marginally affected and affected categories.

Results and discussions

Jute crop map over the study area

Cloud-free Sentinel-2 data of 9 April and 14 May 2020, as mentioned in the "Satellite data used" section, were used for mapping of the jute crop. As per the phenology of jute crop and field observations of BHUVAN JUMP mobile app, jute crop sowing started after the first week of April and attains its peak in the last fortnight. Hence, the agriculture field

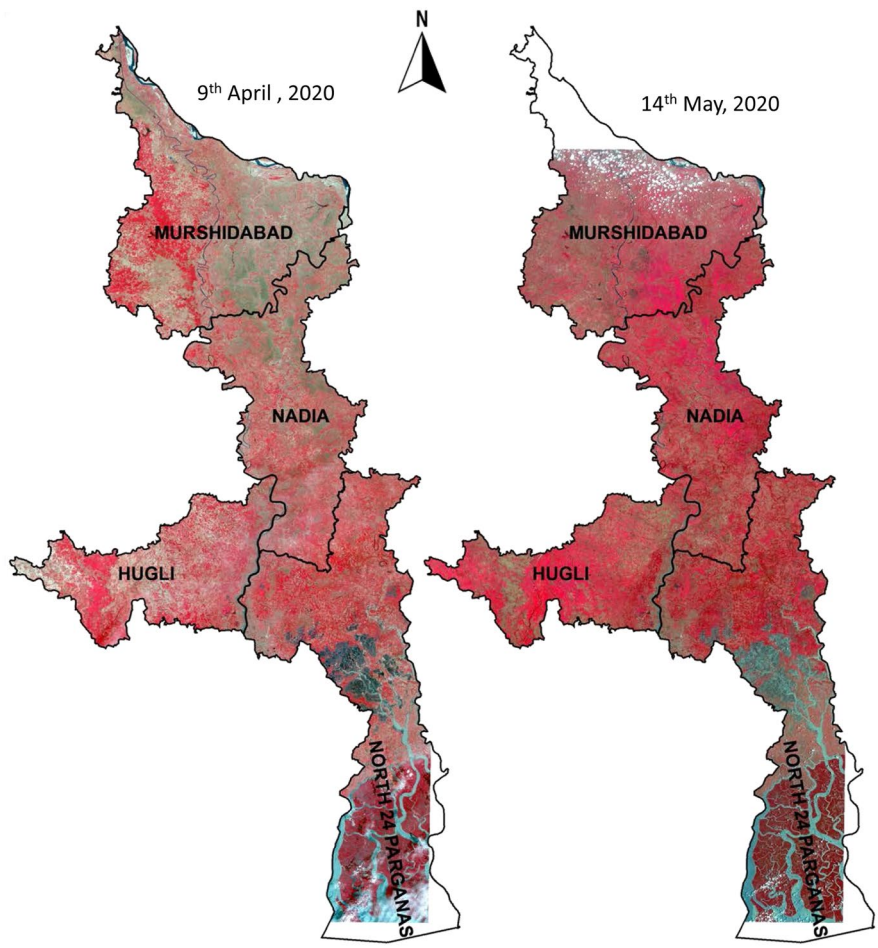

Fig. 7 False color composite of Sentinel-2 images of the study area

would be fallow or with little vegetation (for early sown jute crop) as on 9 April Sentinel-2 image. The spectral signature of these fields has more dominance of soil reflectance than of vegetation. The NDVI value of 9 April over the jute growing areas was found to be low (~0.2). Jute crop attained height of 3–5 ft as on 14 May 2020. So, the soil background was nearly covered by the jute crop and the vegetation signature dominates over the spectral domain. The NDVI values were found to be 0.5 to 0.8 over the jute growing field. Other competing crops, such as *Til* (*Sesamum*) and vegetable showed high NDVI values during 9 April as these were sown/planted during the month of February. The field data points collected over the jute crop area were used to classify the jute crop. Nearly 80% of the data points were randomly selected to develop the jute crop spectral signature, and rest were used for accuracy assessment. In nutshell, the jute crop has successfully been mapped using rule-based classification technique involving the spectral-temporal signature of satellite data and ground truth collected using BHUVAN JUMP mobile app with an accuracy of 85% (Fig. 8).The estimated jute crop areas over the selected districts are presented in Table 2. Total estimated area under the jute crop over the four selected districts was found to be 305,963 ha. Murshidabad district occupies the lion share of it with total area of 136,758 ha followed by Nadia with 100,789 ha. Hooghli and North 24 Paraganas have jute crop area of 34,108 and 34,308 ha respectively.

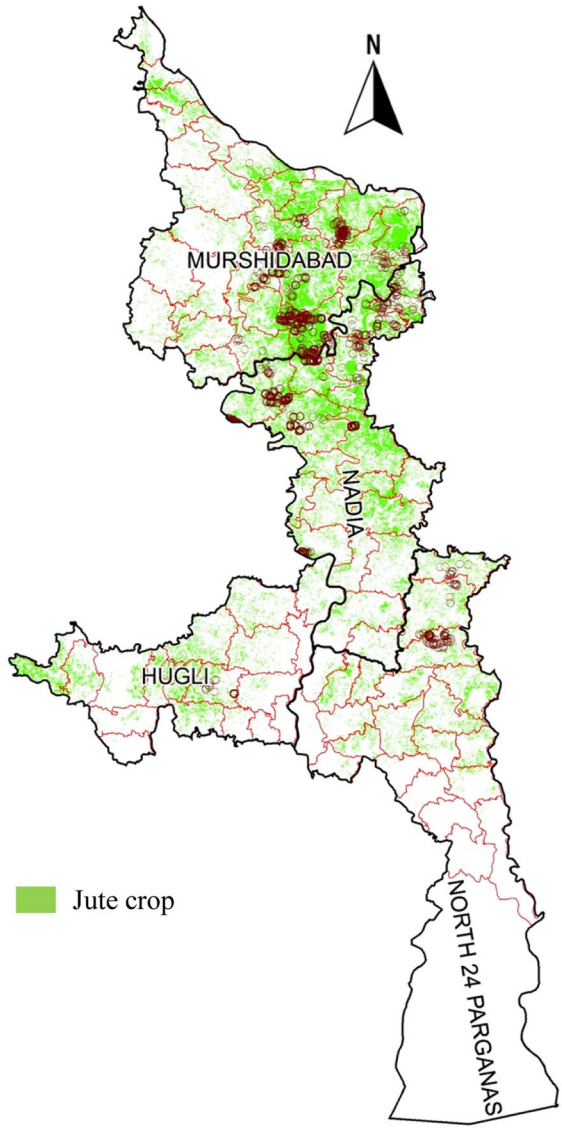

Fig. 8 Satellite-derived jute crop map overlaid with field data

Effect of lodging and water logging on jute crop

The jute crop is grown highly contiguously. All India Network Project on Jute and Allied Fibres recommended row spacing of 22–25 cm for *Corchorus olitorius* and 25–30 cm for *Corchorus capsularis* (Mahapatra et al., 2009). Farmers generally broadcast jute seed (@5–7 kg ha^{-1}), and later thinning operation is done at 30 days after sowing to maintain the recommended plant density. The jute crop attains height of 9–10 ft with a green plant weight yield of 45–50 t ha^{-1} during harvesting. In nutshell, jute crop is a high biomass producing crop grown in high plant density to attain higher height to fetch more fiber. Vertically oriented tall jute crop canopy is vulnerable to water logging and lodging due to high rainfall/cyclonic storm. The jute crop is particularly vulnerable to shear stress and twisting action of the cyclonic storm due to its height. The breakage of stem cause ruptures to the bast fiber and secondary infection. Associated water logging for a week can cause premature senescence, reduction in plant height, basal diameter, ultimately fiber yield loss of 20–60% (Ghorai et al., 2005). In the present study, jute crop was 1 to 1.5-month-old and had attained varying height of 2–5 ft as per the ground information. The taller plant was found to be affected more due to lodging than the smaller one. Hence, jute crop area has been stratified into low,

Table 2 Estimated jute crop area over the selected districts of West Bengal using multi-temporal Sentinel-2 data

Districts	Jute cropped area (ha)
Murshidabad	136,758
Nadia	100,789
24 Paraganas (N)	34,308
Hooghly	34,108

medium, and high vigor based on the NDVI value. Dynamics of backscatter return from these categories were analyzed to derived specific threshold to assess the damage.

Backscattering response to partial flooding and lodging

The wavelength of Sentinel-1 is nearly 5.4 cm and is comparable to the size of some of the jute plant components such as leaves, twigs, and branches, which makes it particularly useful for monitoring jute crop. It also has wide incident angle of nearly 40°, which enables it to interact over longer path length within the crop canopy. The temporal profile of backscattering coefficient in different polarization over a normal jute crop is shown in Fig. 9A. As discussed earlier, the jute crop is grown in highly contiguously and has vertically oriented canopy structure. Hence, VV components of Sentinel-1 data (σ^0_{VV}) interacts more with the vertically oriented jute canopy and the return of it is also found to be more comparatively. The σ^0_{VV} was found to vary from −11 to −7 dB, but it remains invariant in the month of May after the jute crop attains height of 4–5 ft due to saturation of the signal. It is apt to note here that the variation of the σ^0_{VV} was found to be high throughout the time as shown by its high standard deviation values. On the other hand, the cross-polarization component (σ^0_{VH}), which is highly dependent on the volume or random scattering of the crop, found to vary from −20 to −13 dB. As the jute crop attains its above ground biomass, the σ^0_{VH} components increases gradually. At the higher biomass of jute crop, σ^0_{VV} component becomes relatively invariant but the σ^0_{VH} component keeps on increasing with the biomass. As a result, the cross-polarized ratio (CR), i.e., $\sigma^0_{VH}/\sigma^0_{VV}$ also found to increase accordingly. In nutshell, σ^0_{VH} was found to have more dynamic range and sensitive to the crop canopy volume. Similar observations were found by several previous studies (Chauhan et al., 2020a; Shu et al., 2020; Wu et al., 2019).

The super cyclone *Amphan* caused large-scale damage of the jute crop by lodging and partial inundation. The lodging of the crop disrupts the original vertically oriented canopy structure of the jute crop and cause randomness in the field. This randomness causes enhanced volume scattering and the σ^0_{VH} return becomes more. Further, the lodging exposes the below canopy water signature of the partial inundation. The combination of lodging associated with the partial inundation cause double bounce or odd bounce scattering of the RADAR signal. Studies show that σ^0_{VV} and σ^0_{VH} are also sensitive to vegetation-soil interactions, i.e., double bounce effect (Picard et al., 2003). As a result, both σ^0_{VV} and σ^0_{VH} component increases abruptly due to the lodging with partial flooding. The relative change in σ^0_{VV} was smaller than that of σ^0_{VH}.

It is important to note here that the extent of the temporal change in backscattering coefficient depends on the jute crop height. The early sown jute crop which attained higher height (4–5 ft) is more susceptible to lodging due to cyclone and caused relatively higher degree randomness in the field as well as volume scattering (σ^0_{VH}). Late sown jute crops were short in height (1–2 ft) and did not cause the same effect. To account the height/vigor of the jute crop, NDVI value of 14 May Sentinel-2 was classified into different categories based on the frequency distribution of NDVI and ground observed crop information. Three classes of NDVI were made, representing low (< 0.4), medium (0.4–0.6), and high (> 0.6) crop density/height. High and medium categories occupied more than 90% of the jute crop area. Now, based on the post-cyclone ground information of the damaged jute crop, the temporal backscatter signatures of both the polarization were extracted over different NDVI strata. The temporal dynamics of mean backscattering coefficient of co-/cross-polarization along with its standard deviation are presented in Fig. 9B.

It is observed that the σ^0_{VV} is a stronger signal and its value ranging from −11 to −7 dB throughout the jute growing season under the present study

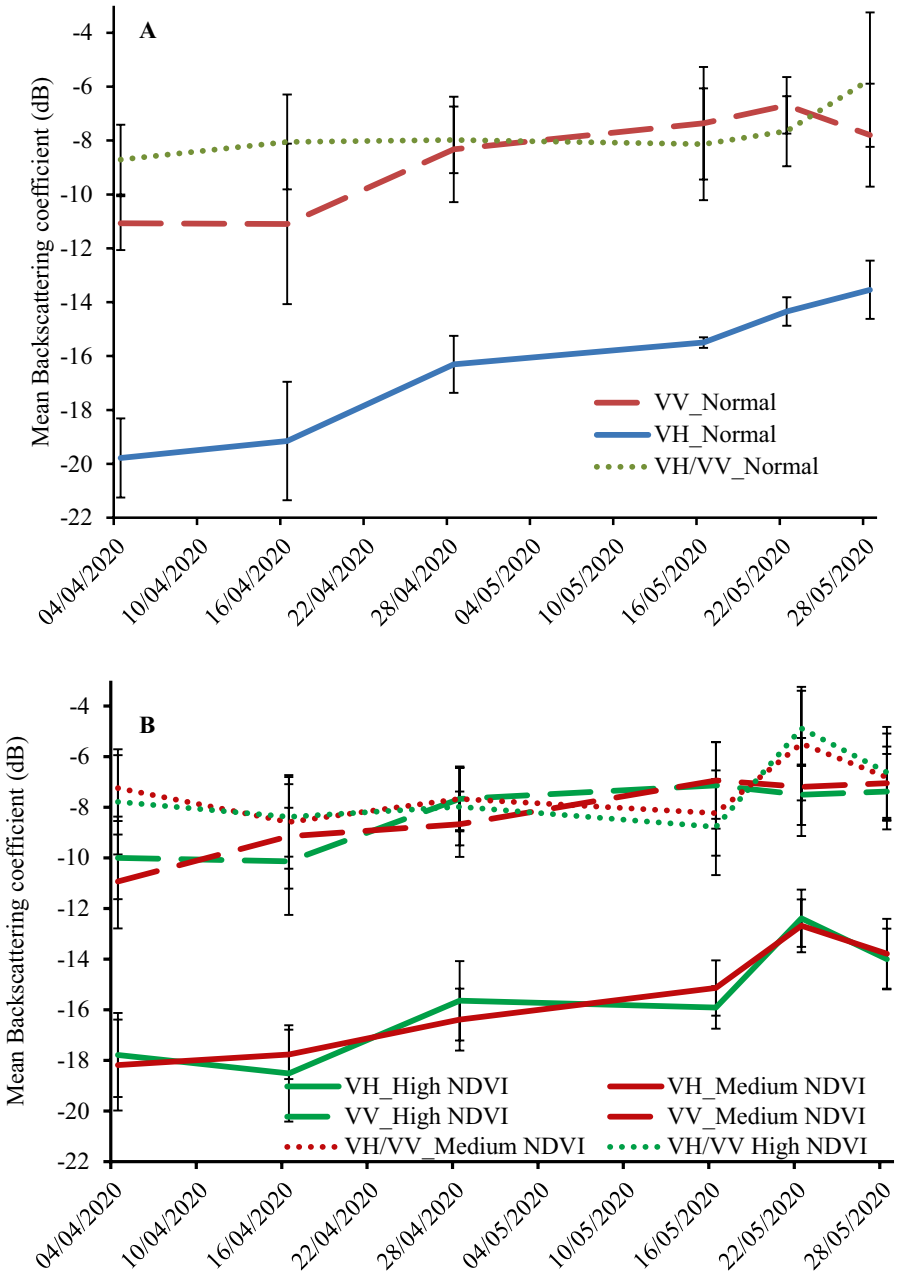

Fig. 9 Temporal profile of backscattering coefficient of Sentinel-1 over **A** normal and **B** affected jute crop

(Fig. 9B). It became invariant or saturated in the higher biomass of jute crop during May month. The σ^0_{VH} was found to increase from −18 to −13 dB as the crop grows. The increase was relatively stable with less fluctuation unlike σ^0_{VV} or CR ($\sigma^0_{VH}/\sigma^0_{VV}$). Importantly, sharp increase in σ^0_{VH} was observed between 16 May (pre-event) and 22 May (post-event) observations. It can be assumed that the increase of biomass and height of the crop from 16 to 22 May was minimal. So, this sudden rise in backscattering coefficient is attributed to the lodging and partial inundation of the jute crop. The cross-polarization

ratio (CR) followed the same pattern as that of σ^0_{VH} with more fluctuations. The change in backscatter values between 22 and 28 May actually denotes the post-event recovery. Within a window of 6 days, the water may have subsided from some places and the jute crop recovered from lodging, at least partially. This may reduce the degree of randomness in the field and make the jute canopy aligned to the vertical plane, at least partially. As an effect, the cross-polarized backscatter difference (σ^0_{VH}) has come down to near-normalcy showing recovery from lodging (Fig. 9B). In the present study, post-cyclonic damage and recovery both are considered to assess the affected area.

Statistics of backscattering response over the affected area

Post-event field observations of affected the jute crop fields were used to generate the signature of backscattering coefficient values of Sentinel-1 data of 16, 22, and 28 May 2020. The 16 and 22 May data pertains to pre-cyclonic and post-cyclonic condition, respectively; 28 May represents the post-event recovery of the jute crop. NDVI values of Sentinel-2 data was used to stratify the jute crop vigor into three classes high (NDVI > 0.6) and medium (NDVI = 0.4–0.6) and low (NDVI < 0.4). Mean and standard deviation values of the backscatter difference of 22 May and 16 May, referred as $\Delta\sigma^0$ in VV and VH polarization along with the cross-polarization ratio ($\Delta CR = \Delta\sigma^0_{VH}/\Delta\sigma^0_{VV}$) at different NDVI ranges, are presented in Table 3. Likewise, the backscatter difference of 22 and 28 May, referred as $\delta\sigma^0$ in VV and VH polarization along with the cross-polarization ratio ($\delta CR = \delta\sigma^0_{VH}/\delta\sigma^0_{VV}$) at different NDVI ranges were also presented in Table 3.

The $\triangle\sigma^0_{VV}$ values were found to be low and remain invariant across the NDVI ranges. The σ^0_{VV}, as discussed in the previous section, saturates earlier as the crop attains moderate to high aboveground biomass. The $\triangle\sigma^0_{VH}$ was found to be high, i.e., ~ 3.5 dB for high NDVI region. For medium and low vigor crop, it was 2.6 dB and 0.59 dB, respectively. The standard deviation was found to be relatively lower. The CR is influenced by both $\triangle\sigma^0_{VH}$ and $\triangle^0_{VV}$. As $\triangle\sigma^0_{VV}$ remained invariant, it followed the same trend as that of $\triangle\sigma^0_{VH}$ with higher standard deviation. Hence, $\triangle\sigma^0_{VH}$ was used to characterize the lodging and partial inundation of jute crop. Similarly, the response of $\delta\sigma^0_{VH}$ (considering its mean and SD) was found to be suitable to characterize the post-damage recovery of jute crop. Higher value of $\delta\sigma^0_{VH}$ denotes reduced volume scattering, meaning reduction in the randomness/lodging of the jute canopy due to post-cyclonic recovery.

Decision matrix to assess affected jute area

Based on the backscattering response patterns between (a) 16 and 22 May indicating damage phase and (b) 22 and 28 May indicating recovery phase over different crop vigor classes, decision rules were formulated to map the affected jute crop area. As discussed in the previous section, the cross-polarized backscatter response was found to be sensitive to the lodging of the crop and also relatively stable. Hence, mean and standard deviation values of $\triangle\sigma^0_{VH}$ and $\delta\sigma^0_{VH}$ at different NDVI region was considered to formulate a decision matrix to characterize and map the affected jute crop area as shown in Fig. 10. The high value of $\triangle\sigma^0_{VH}$ denotes increase in volume scattering due to increase in randomness of the canopy structure due to lodging of jute crop. At the same time, high value of $\delta\sigma^0_{VH}$ means decrease in the randomness of the canopy due to recovery of the crop. Hence, high value of $\triangle\sigma^0_{VH}$ in combination with low value of $\delta\sigma^0_{VH}$ pertains to high degree of damage of jute crop and vice versa.

The criteria, as shown in Fig. 10, are fixed based on the mean value of $\triangle\sigma^0_{VH}$ and $\delta\sigma^0_{VH}$ along with its variations to achieve acceptable accuracy of the classified jute affected area. It is important to mention here that, the logic of fixing the threshold is data driven and can accommodate changes in crop season, crop type, and crop stages, etc. The criteria are fixed for high and moderate categories of NDVI/crop vigor. For low NDVI region, the effect of crop canopy is minimal. Hence, it is treated as nearly bare soil and criterion is fixed based on flooded field condition as mentioned below.

In case of high crop vigor (NDVI > 0.6),

Table 3 Statistics of the backscatter differences over different crop vigor classes (based on NDVI) of the affected jute crop area; SD = standard deviation; parameters used in decision matrix are highlighted as bold.

	Difference σ^0 of 22 and 16 May 2020 in dB (pre- and post-event; damage)					
NDVI	$\overline{\triangle\sigma^0_{VV}}$	SD of $\triangle\sigma^0_{VV}$	$\overline{\triangle\sigma^0_{VH}}$	SD of $\triangle\sigma^0_{VH}$	$\overline{\triangle CR}$	SD of ΔCR
High	−0.37	1.78	**3.53**	**0.85**	3.53	0.85
Medium	−0.30	1.69	**2.61**	**1.30**	2.92	2.35
Low	0.33	1.78	**0.59**	**0.35**	0.26	1.89
	Difference σ^0 of 22 and 28 May 2020 (post-event recovery)					
NDVI	$\overline{\delta\sigma^0_{VV}}$	SD of $\delta\sigma^0_{VV}$	$\overline{\delta\sigma^0_{VH}}$	SD of $\delta\sigma^0_{VH}$	$\overline{\delta CR}$	SD of δCR
High	−0.12	1.78	**1.61**	**1.68**	1.74	2.22
Medium	−0.29	2.21	**1.07**	**1.37**	1.36	2.62
Low	1.54	1.28	**1.50**	**0.90**	−0.05	0.38

– If $\triangle\sigma^0_{VH}$> 4 dB and $\delta\sigma^0_{VH}$<2.5 dB, the jute crop is affected.
– If 3.5 dB ≥ $\triangle\sigma^0_{VH}$ ≤ 4 dB and $\delta\sigma^0_{VH}$<2 dB, the jute crop is marginally affected.
– Otherwise, jute crop is normal

In case of moderate crop vigor (0.4 > NDVI ≤ 0.6),

– If $\triangle\sigma^0_{VH}$ > 3 dB and $\delta\sigma^0_{VH}$ < 1.5 dB, the jute crop is affected
– If 2.5 dB ≥ $\triangle\sigma^0_{VH}$ ≤ 3 dB and $\delta\sigma^0_{VH}$ < 1.5 dB, the jute crop is marginally affected.
– Otherwise, jute crop is normal

Low NDVI region did not show sensitivity to the cross-polarization components as the crop biomass and height is very low. Hence, it is simply treated as open water condition and classified as follows:

– If, σ^0_{VV} < −15 dB both on 22 and 28 May, it is affected.
– If σ^0_{VV} < −15 dB on 22 but not in 28 May, it is marginally affected.
– Otherwise, jute crop is normal.

Mapping of affected jute crop area

Based on the decision matrix as described earlier, jute crop area affected or marginally affected due to *Amphan* was mapped over the selected districts and

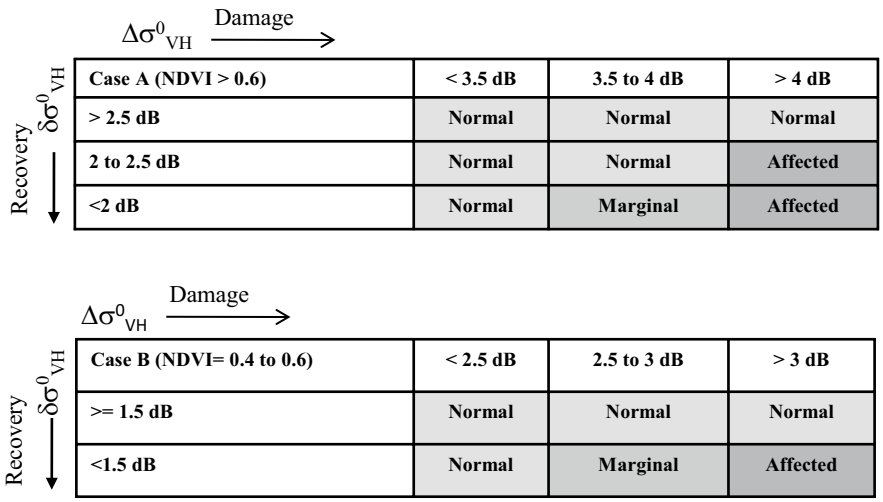

Fig. 10 Decision matrixes for delineating affected area of jute crop. **A** High crop vigor. **B** Moderate crop vigor

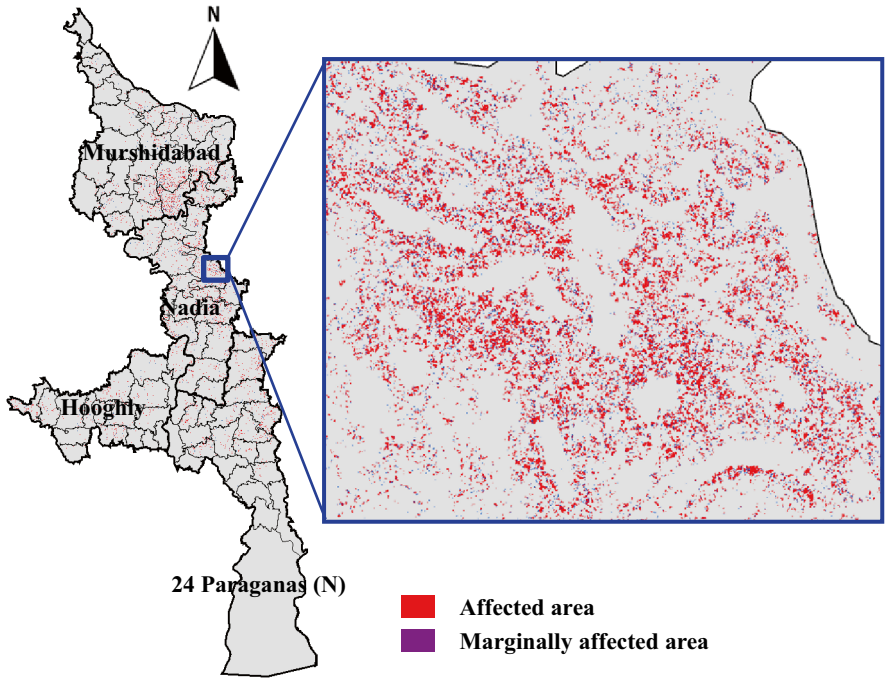

Fig. 11 Geospatial map showing affected jute crop area due to *Amphan*

presented in Fig. 11. Accuracy assessment of classified map was done using the post-cyclonic field observations (excluding the points used for signature generation) and presented in Table 4. High user accuracy (> 85%) is observed for all the classes, whereas the producer accuracy was found to be high (94.74%) for normal class, followed by 76.36% for affected classes and 68.57% for marginally affected class. Overall accuracy was found to be 84.32% with kappa coefficient of 0.74.

Out of total jute area of 305,963 ha over the selected districts, nearly 12.5%, i.e., 38,119 ha was affected/marginally affected due to *Amphan*. These areas are mainly distributed in the southern part of Murshidabad, North-eastern part of Nadia, Northern part of 24 Paraganas (N) and middle region of Hooghli district. The district-wise jute cropped areas affected/marginally affected due to *Amphan* are presented in Table 5. North 24 Paraganas is the most affected district with 19.5% of total jute area under affected category. It is followed by Nadia (15%), Hooghli (14%), and Murshidabad (8.5%).

Table 4 Accuracy assessment of the classified jute area affected due to *Amphan*

Classes	Producer accuracy (%)	User accuracy (%)
Affected	76.36	89.36
Marginally affected	68.57	85.11
Normal	94.74	85.71

The total affected jute cropped area due to cyclone in each of the block in the selected districts was calculated. The geospatial map showing block-wise spatial distribution of the total affected jute area is presented in Fig. 12. Highly affected blocks are found to be distributed in the southern parts of Murshidabad, North eastern Nadia, northern parts of 24 Paraganas (N). Nawda, Hariharpara, Domkal, and Belganga I and II of Murshidabad; Chapra, Haskhali, Nakashipara, Krishnanagar, Karimpur-II, and Tehatta-I of Nadia; Bongaon, Swarupnagar, Bagda, and Baduria of North 24 Paraganas; and Goghat of Hooghli were found to have high proportion of jute area affected by the cyclone *Amphan*. The spatial distributions of the affected blocks are in coherence with the cyclone path and the dominating area growing jute crop.

Table 5 District-wise jute area affected due to cyclone *Amphan*

Districts	Jute crop area (ha)	Affected area: A (ha)	Marginally affected area: M (ha)	Total area: A + M (ha)	% of (A + M) to jute crop area
Murshidabad	136,758	7538	4090	11,628	8.5
Nadia	100,789	9767	5229	14,996	15.0
24 Paraganas (N)	34,308	4620	2038	6658	19.5
Hooghli	34,108	3099	1738	4837	14.0

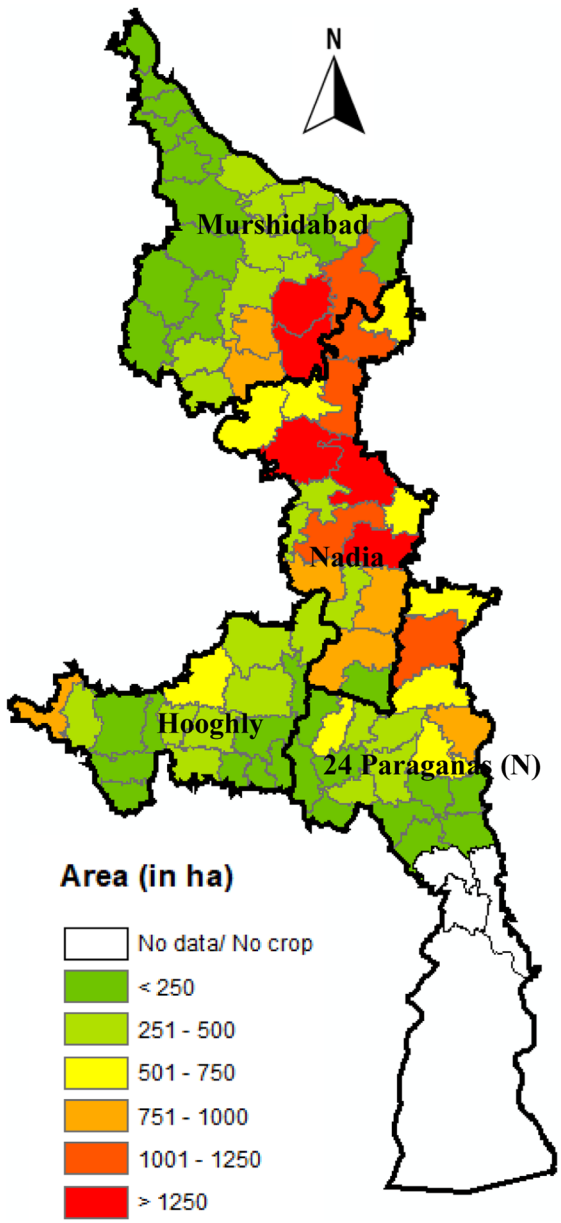

Fig. 12 Block-wise distribution of affected jute crop area

Conclusions

The present study has successfully demonstrated the scope of multi-platform, multi-temporal satellite data for objective assessment of jute crop area affected by *Amphan* cyclone (20 May 2020) in parts of West Bengal. Extensive ground truth data, collected over the jute crop before and after the disaster, revealed that the cyclone caused significant damage by lodging and partial/full inundation of the crop. Pre-event cloud-free Sentinel-2 optical data (9 April and 14 May) along with the ground information were used to map the jute crop of affected districts (Murshidabad, Nadia, North 24 Paraganas, and Hooghli) of West Bengal with over all accuracy of 85%. This jute crop map was further used to assess the temporal response of the backscatter return of Sentinel-1 in dual polarization (VV, VH) and cross-polarization ratio ($\sigma^0_{VH}/\sigma^0_{VV}$) based on the post-event ground truth data. Three dates of Sentinel-1 SAR data were used to achieve the desired objectives; 16 May (pre-event), 22 May (post-event), and 28 May (post-event recovery). The cross-polarized return (σ^0_{VH}) is sensitive to volume/random scattering of crop canopy. The sudden change in the canopy structure, due to crop lodging associated with partial flooding, has been picked up well by the temporal change of cross-polarized return. The cross-polarized backscatter difference of pre- and post-event ($\triangle\sigma^0_{VH}$), i.e., σ^0_{VH} of 22 May $-\sigma^0_{VH}$ of 16 May, was found to be 2.5 dB or more over the affected jute crop depending on the crop vigor (NDVI). At the same time, post-event recovery represented by $\delta\sigma^0_{VH}$ (i.e., σ^0_{VH} of 22 May $-\sigma^0_{VH}$ of 28 May) was found to be 1.5 dB or more for recovered crop. Hence, the jute crop area was stratified into low, medium, and high vigor using the NDVI value derived from Sentinel-2 data of 14 May. The mean and variations of $\triangle\sigma^0_{VH}$ and $\delta\sigma^0_{VH}$ over affected area across different jute crop strata were derived and used to fix threshold for different categories of the affected area. Decision matrixes were prepared based on $\triangle\sigma^0_{VH}$ and

$\delta\sigma^0_{VH}$ for each stratum of jute crop to classify the area into affected, marginally affected and normal. Overall accuracy of the classified map was found to be 84.32% with Kappa coefficient of 0.74. Nearly 12.5% of the jute cropped area of the selected districts, i.e., 38,119 ha, was found to be affected/marginally affected due to *Amphan* and mainly distributed in the southern part of Murshidabad, northeastern part of Nadia, northern part of 24 Paraganas (N), and middle region of Hooghli district. Geospatial map of blocks (sub-district) level affected jute crop area was also prepared to facilitate informed decision making. The study has thus established a scientific basis for operational assessment of crop area affected due to such calamities. The information may act as an input for relief management and crop insurance value chain.

Acknowledgements We are grateful to IMD for providing daily weather data which are essential for such crop damage assessment studies. Efforts of the officials of Jute Corporation of India and National Jute Board are duly acknowledged for providing near real time field data using *BHUVAN JUMP* mobile app. Valuable comments of the editor and reviewers significantly improved the manuscript.

Author contribution The first author conceived the idea and analyzed the data and written the manuscript; the second author analyzed the data and made the figures and tables; the third and fourth authors reviewed the results and manuscript for finalization; and the fifth author was responsible for overall guidance.

Availability of data and material All the data are free of cost and are in open domain.

Declarations

Conflict of interest The authors declare no competing interests.

References

Baker, C. J., Sterling, M., & Berry, P. (2014). A generalised model of crop lodging. *Journal of Theoretical Biology, 363*, 1–12. https://doi.org/10.1016/j.jtbi.2014.07.032

Berry, P. M., Sterling, M., Spink, J. H., Baker, C. J., Sylvester-Bradley, R., Mooney, S. J., Tams, A. R., & Ennos, A. R. (2004). Understanding and reducing lodging in cereals. *Advances in Agronomy, 84*(04), 215–269. https://doi.org/10.1016/S0065-2113(04)84005-7

Bouman, B. A. & van Kasteren, H. W. (1990a). Ground-based X-band (3-cm wave) radar backscattering of agricultural crops. I. Sugar beet and potato; backscattering and crop growth. *Remote Sensing of Environment*, *34*(2), 93–105. https://doi.org/10.1016/0034-4257(90)90101-Q

Bouman, B. A. & van Kasteren, H. W. (1990b). Ground-based X-band (3-cm wave) radar backscattering of agricultural crops. II. Wheat, barley, and oats; the impact of canopy structure. *Remote Sensing of Environment, 34*(2), 107–119. https://doi.org/10.1016/0034-4257(90)90102-R

Bouman, B. A. M. (1991). Crop parameter estimation from ground-based X-band (3-cm wave) radar backscattering data. *Remote Sensing of Environment, 37*(3), 193–205. https://doi.org/10.1016/0034-4257(91)90081-G

Brune, P. F., Baumgarten, A., McKay, S. J., Technow, F., & Podhiny, J. J. (2018). A biomechanical model for maize root lodging. *Plant and Soil, 422*(1–2), 397–408. https://doi.org/10.1007/s11104-017-3457-9

Chapman, S. C., Merz, T., Chan, A., Jackway, P., Hrabar, S., Dreccer, M. F., Holland, E., Zheng, B., Ling, J. T., & Jimenez-Berni, J. (2014). Pheno-copter: A low-altitude, autonomous remote-sensing robotic helicopter for high-throughput field-based phenotyping. *Agronomy, 4*(2), 279–301. https://doi.org/10.3390/agronomy4020279

Chauhan, S., Darvishzadeh, R., Boschetti, M., Pepe, M., & Nelson, A. (2019). Remote sensing-based crop lodging assessment: Current status and perspectives. *ISPRS Journal of Photogrammetry and Remote Sensing, 151*, 124–140. https://doi.org/10.1016/j.isprsjprs.2019.03.005

Chauhan, S., Darvishzadeh, R., Boschetti, M., & Nelson, A. (2020a). Estimation of crop angle of inclination for lodged wheat using multi-sensor SAR data. *Remote Sensing of Environment, 236*, 111488. https://doi.org/10.1016/j.rse.2019.111488

Chauhan, S., Darvishzadeh, R., Lu, Y., Boschetti, M., & Nelson, A. (2020b). Understanding wheat lodging using multi-temporal Sentinel-1 and Sentinel-2 data. *Remote Sensing of Environment, 243*, 111804. https://doi.org/10.1016/j.rse.2020.111804

Chen, J., Li, H., & Han, Y. (2016). Potential of RADARSAT-2 data on identifying sugarcane lodging caused by typhoon. In: Fifth International Conference on Agro-Geoinformatics (Agro-Geoinformatics) IEEE (pp. 1–6). https://doi.org/10.1109/Agro-Geoinformatics.2016.7577665

Chu, T., Starek, M. J., Brewer, M. J., Murray, S. C., & Pruter, L. S. (2017). Assessing lodging severity over an experimental maize (Zea mays L.) field using UAS images. *Remote Sensing*, *9*(9), 923. https://doi.org/10.3390/rs9090923

Constantinescu, C. A., Herbei, M. V., Manea, D., & Sala, F. (2017). Analysis of some deficiencies in crops of wheat and barley based on terrestrial and aerial images. *Research Journal of Agricultural Science*, *49*(1). https://www.rjas.ro/paper_detail/2384

ESA Standard Document. (2015). SENTINEL-2 User Handbook. *European Space Agency*. https://sentinel.esa.int/documents/247904/685211/Sentinel-2_User_Handbook

Ezequiel, C. A. F., Cua, M., Libatique, N. C., Tangonan, G. L., Alampay, R., Labuguen, R. T., Favila, C. M., Honrado, J. L. E., Canos, V., Devaney, C., & Loreto, A. B. (2014). UAV aerial imaging applications for post-disaster assessment, environmental management and infrastructure development. In 2014 International Conference on Unmanned Aircraft Systems (ICUAS) May. IEEE (pp. 274–283). https://doi.org/10.1109/ICUAS.2014.6842266

Ghorai, A. K., Bhattacharjee, A. K., Saha, S., Rao, P. V., & Bandopadhyay, A. K. (2005). Impact of waterlogging on yield and quality of tossa jute (Corchorus olitorius). *Indian Journal of Agronomy*, *50*(4), 320–323. https://www.indianjournals.com/ijor.aspx?target=ijor:ija&volume=50&issue=4&article=021

Han, D., Yang, H., Yang, G., & Qiu, C. (2017). Monitoring model of corn lodging based on Sentinel-1 radar image. In: SAR in Big Data Era: Models, Methods and Applications (BIGSARDATA), Beijing, 2017, pp. 1–5. https://doi.org/10.1109/BIGSARDATA.2017.8124928

Islam, M. S., Peng, S., Visperas, R. M., Ereful, N., Bhuiya, M. S. U., & Julfiquar, A. W. (2007). Lodging-related morphological traits of hybrid rice in a tropical irrigated ecosystem. *Field Crops Research, 101*(2), 240–248. https://doi.org/10.1016/j.fcr.2006.12.002

Liu, Z., Li, C., Wang, Y., Huang, W., Ding, X., Zhou, B., Wu, H., Wang, D., & Shi, J. (2011). Comparison of spectral indices and principal component analysis for differentiating lodged rice crop from normal ones. In International Conference on Computer and Computing Technologies in Agriculture (pp. 84–92). Springer, Berlin, Heidelberg. https://doi.org/10.1007/978-3-642-27278-3_10

Liu, H. Y., Yang, G. J., Zhu, H. C. (2014). The extraction of wheat lodging area in UAV's image used spectral and texture features. *Applied Mechanics and Materials 651*, 2390–2393. https://doi.org/10.4028/www.scientific.net/AMM.651-653.2390

Mahapatra, B. S., Mitra, S., Sinha, M. K., & Ghorai, A. K. (2009). Research and development in jute (*Corchorus* sp.) and allied fibres in India–A review. *Indian Journal of Agronomy*, *54*(4), 361–373. https://www.indianjournals.com/ijor.aspx?target=ijor:ija&volume=54&issue=4&article=002

Mi, C., Zhang, X., Li, S., Yang, J., Zhu, D., & Yang, Y. (2011). Assessment of environment lodging stress for maize using fuzzy synthetic evaluation. *Mathematical and Computer Modelling, 54*(3–4), 1053–1060. https://doi.org/10.1016/j.mcm.2010.11.035

Nebiker, S., Annen, A., Scherrer, M., & Oesch, D. (2008). A light-weight multispectral sensor for micro UAV—Opportunities for very high resolution airborne remote sensing. *The International Archives of The Photogrammetry, Remote Sensing and Spatial Information Sciences*, *37*(B1), 1193–1199. https://citeseerx.ist.psu.edu/viewdoc/download?doi=10.1.1.151.820&rep=rep1&type=pdf

Ogden, R. T., Miller, C. E., Takezawa, K., & Ninomiya, S. (2002). Functional regression in crop lodging assessment with digital images. *Journal of Agricultural, Biological, and Environmental Statistics, 7*(3), 389–402. https://doi.org/10.1198/108571102339

Picard, G., Le Toan, T., & Mattia, F. (2003). Understanding C-band radar backscatter from wheat canopy using a multiple-scattering coherent model. *IEEE Transactions on Geosciences and Remote Sensing, 41*(7), 1583–1591. https://doi.org/10.1109/TGRS.2003.813353

Piñera-Chavez, F. J., Berry, P. M., Foulkes, M. J., Molero, G., & Reynolds, M. P. (2016). Avoiding lodging in irrigated spring wheat. II. Genetic variation of stem and root structural properties. *Field Crops Research, 196*, 64–74. https://doi.org/10.1016/j.fcr.2016.06.007

Pinthus, M. J. (1974). Lodging in wheat, barley, and oats: The phenomenon, its causes, and preventive measures. *Advances in Agronomy, 25*, 209–263. https://doi.org/10.1016/S0065-2113(08)60782-8

Sakamoto, T., Shibayama, M., Takada, E., Inoue, A., Morita, K., Takahashi, W., Miura, S., & Kimura, A. (2010). Detecting seasonal changes in crop community structure using day and night digital images. *Photogrammetric Engineering & Remote Sensing*, *76*(6), 713–726. https://doi.org/10.14358/PERS.76.6.713

Shu, M., Zhou, L., Gu, X., Ma, Y., Sun, Q., Yang, G., & Zhou, C. (2020). Monitoring of maize lodging using multi-temporal Sentinel-1 SAR data. *Advances in Space Research, 65*(1), 470–480. https://doi.org/10.1016/j.asr.2019.09.034

Wu, W., & Ma, B. L. (2016). A new method for assessing plant lodging and the impact of management options on lodging in canola crop production. *Scientific Reports, 6*, 31890. https://doi.org/10.1038/srep31890

Wu, W., Wang, W., Meadows, M. E., Yao, X., & Peng, W. (2019). Cloud-based typhoon-derived paddy rice flooding and lodging detection using multi-temporal Sentinel-1&2. *Frontiers of Earth Science, 13*(4), 682–694. https://doi.org/10.1007/s11707-019-0803-7

Yang, H., Chen, E., Li, Z., Zhao, C., Yang, G., Pignatti, S., Casa, R., & Zhao, L. (2015). Wheat lodging monitoring using polarimetric index from RADARSAT-2 data. *International Journal of Applied Earth Observation and Geoinformation, 34*, 157–166. https://doi.org/10.1016/j.jag.2014.08.010

Yang, M. D., Huang, K. S., Kuo, Y. H., Tsai, H. P., & Lin, L. M. (2017). Spatial and spectral hybrid image classification for rice lodging assessment through UAV imagery. *Remote Sensing, 9*(6), 583. https://doi.org/10.3390/rs9060583

Zhang, C., Walters, D., & Kovacs, J. M. (2014). Applications of low altitude remote sensing in agriculture upon farmers' requests–a case study in northeastern Ontario, Canada. *PLoS One, 9*(11), e112894. https://doi.org/10.1371/journal.pone.0112894

Zhao, L., Yang, J., Li, P., Shi, L., & Zhang, L. (2017). Characterizing lodging damage in wheat and canola using Radarsat-2 polarimetric SAR data. *Remote Sensing Letters, 8*(7), 667–675. https://doi.org/10.1080/2150704X.2017.1312028

Zhu, G., Li, G., Wang, D., Yuan, S., & Wang, F. (2016). Changes in the lodging-related traits along with rice genetic improvement in China. *PLoS One, 11*(7), e0160104. https://doi.org/10.1371/journal.pone.016010